Contents lists available at SciOpen

Food Science and Human Wellness

journal homepage: https://www.sciopen.com/journal/2097-0765

China Food Publishing Co.

Physicochemical characterization of *Dendrobium officinale* polysaccharides and regulation of immune homeostasis in sub-health mice based on the CD4$^+$-Th17/Treg immunity axis

Bo Li[a,b,1], Zehua Zhang[a,b,1], Linnan Zhang[a,b,1], Xinglishang He[a,b], Haoru Guan[a,b], Ning Wang[a,b], Yingjie Dong[c], Mei Rong[a,b], Jiujie Jia[a,b], Tingting Chen[a,b], Zhiyuan Li[a,b], Guiyuan Lü[c,*], Suhong Chen[a,b,*]

[a] *Collaborative Innovation Center of Yangtze River Delta Region Green Pharmaceuticals, Zhejiang University of Technology, Hangzhou 310014, China*
[b] *Zhejiang Provincial Key Laboratory of TCM for Innovative R&D and Digital Intelligent Manufacturing of TCM Great Health Products, Huzhou 313200, China*
[c] *College of Pharmaceutical Science, Zhejiang Chinese Medical University, Hangzhou 310053, China*

ARTICLE INFO

Article history:
Received 5 January 2024
Received in revised form 14 February 2024
Accepted 11 April 2024

Keywords:
Dendrobium officinale
Polysaccharides
Intestinal barrier
Immunity
Sub-healthy
CD4$^+$-Th17/Treg

ABSTRACT

The aim of this study was to investigate the role of *Dendrobium officinale* crude polysaccharides (DOPS) and *D. officinale* purified polysaccharides (DOPS100) in attenuating immune dysfunction in subfertile mice. The results of the study revealed several noteworthy findings. First, DOPS and DOPS100 treatments led to significant improvement in weight gain and reversal of fatigue-related behaviors compared to the normal group. Second, both DOPS and DOPS100 showed effectiveness in reducing immune organ swelling, modulating immunoglobulin A (IgA) and immunoglobulin M (IgM) levels, and restoring complement (C3c and C4) levels. In addition, they demonstrated a significant ability to enhance the integrity of the intestinal mechanical barrier by differentially upregulating the tight junction proteins Occludin and Zonula occludens 1 (ZO-1). In addition, it was found that DOPS100 specifically enhanced the CD4$^+$-T helper 17 cell (Th17)/regulatory T cell (Treg) immune axis in the gut, as evidenced by increased expression of forkhead box protein 3 (Foxp3) as well as decreased expression of retinoic acid receptor-related orphan receptor γt (RORγt), and further modulation of interleukin 10 (IL-10), interleukin 22 (IL-22), and interleukin 17A (IL-17A) expression levels of inflammatory factors. These findings collectively suggest that DOPS100 holds significant potential in improving sub-healthy status by repairing the intestinal barrier, restoring local immune homeostasis, and activating the intestinal immune regulatory network. The study's outcomes provide valuable insights into the therapeutic implications of DOPS and DOPS100 in addressing immune dysfunction in sub-healthy conditions.

1. Introduction

The World Health Organization (WHO) reports that in the current society, due to rapid societal changes prevail, many factors contribute to health challenges, including unhealthy dietary habits, insufficient physical activity, irregular work schedules, inadequate rest, sleep deprivation, mental stress, high levels of psychological pressure, and prolonged negative emotions[1-2]. Recent studies have reported that long-term unhealthy dietary habits pose a significant risk to public health, impairing various bodily systemic functions via multiple pathways[3-4]. A global survey conducted by the WHO reported that only 5% of the population is considered truly healthy, with 20% is classified as sick and a significant 75% categorized as being in suboptimal health conditions. While individuals with a suboptimal

[1] Co-first authors.
[*] Corresponding authors.
E-mail addresses: zjtcmlgy@163.com (G.Y. Lü); chensuhong@aliyun.com (S.H. Chen)
Peer review under responsibility of Beijing Academy of Food Sciences.

SciOpen Publishing services by Tsinghua University Press

http://doi.org/10.26599/FSHW.2024.9250268

health condition may not fulfill specific clinical diagnostic criteria for a particular illness, their physical and psychological symptoms warrant serious attention and proactive intervention. Hence, the prevention and management of suboptimal health conditions should be closely prioritized.

The intestine, the largest immune organ in the human body, directly affects the health level of the body. Dysbiosis, local immune dysfunction, and increased intestinal mucosal permeability can facilitate the entry of intestinal pathogens into the bloodstream, triggering various chronic inflammations and compromising immune function, thereby contributing to a suboptimal health state. Several previous studies have shown that intestinal T-cell immune homeostasis plays a crucial role in mediating the occurrence and development of suboptimal health related diseases. Intestinal T cells including $CD8^+$ and $CD4^+$ subsets, primarily consist of T helper 1 cells (Th1), T helper 2 cells (Th2), T helper 17 cells (Th17), and regulatory T cell (Treg) populations. Th17 and Treg, the most abundant $CD4^+$ T cell subsets in mucosal tissue, are crucial for maintaining immune homeostasis and preventing excessive immune responses. Dysregulation of Th17 and Treg can contribute to the development of autoimmune diseases[5]. Cytokines, such as interleukin (IL)-10, produced by Treg according to traditional Chinese medicine, play a privotal role in promoting Treg tolerance. IL-10-deficient mice are more susceptible to spontaneous colonic inflammation, leading to exacerbation of systemic immune dysfunction[6].

Dendrobium officinale, extensively used in traditional Chinese medicine, has been found to offer various health benefits, such as immunoenhancement, antitumor activity, gastrointestinal regulation, hypoglycemic effects, and blood pressure reduction. Complementary medicine approaches, such as herbal formulations, can be used as safer adjunct interventions for suboptimal health[7-10]. Traditional Chinese medicine cannot be separated from its core active ingredients[11]. Polysaccharides are major components of *D. officinale*, which possess pharmacological activities[12]. The stem polysaccharide of *D. officinale* can modulate the immune response in immunosuppressed and healthy mice. They regulate splenic proliferation, balance splenic lymphocyte subpopulations, increase serum immunoglobulin M (IgM), immunoglobulin G (IgG), hemolysin levels, and increase peritoneal macrophage phagocytosis in healthy individuals[13]. Additionally, polysaccharides in the leaves of *D. officinale* possess anti-inflammatory properties[14]. Moreover, *D. officinale* polysaccharides are consumed orally. However, their high molecular weights and unique glycosidic linkages make absorption into the bloodstream through the gastrointestinal tract challenging. Therefore, these polysaccharides may exert their immunomodulatory effects by directly interacting with the intestinal mucosal immune system[15-16]. Furthermore, a national herbal beverage containing *D. officinale* crude polysaccharides (DOPS) has been approved by the State Administration of Market Supervision and Administration as an immune-modulating functional food. It can modulate the immune response in cyclophosphamide (CTX)-induced immunosuppressed mice by restoring intestinal barrier function and regulating dysbiosis[17]. *D. officinale* leaf polysaccharides can alleviate gut barrier damage and inflammation[18]. Xie et al.[16] reported that DOP can effectively change intestinal mucosal structures to modulate intestinal mucosal immune activity.

While these studies highlight the immunomodulatory properties of polysaccharides, the molecular mechanisms underlying these processes are yet to be elucidated. Notably, suboptimal health can have adverse effects on the body. For instance, suboptimal health factors can increase intestinal permeability and downregulate the expression of YWHAZ (tyrosine 3-monooxygenase/tryptophan 5-monooxygenase)[19]. Furthermore, a high-fat diet can compromise immune function at the intestinal and systemic levels, potentially increasing the risk of cancer[20]. Therefore, addressing suboptimal health and implementing effective interventions to improve overall well-being is crucial.

In the present study, we aimed to address current limitations through structured investigation into DOPS, which are hypothesized to be bioactive fractions. Using chromatography techniques, we initially purified the candidate polysaccharide (DOPS100). Subsequently, we focused on characterizing its structure and evaluating its therapeutic effects in an over-consumption of alcohol and high sugar and fat diet (ACHSFDs)-fed suboptimal health mice. Our results indicate that DOPS100 stimulates intestinal immune homeostasis, tight junction protein levels, and anti-inflammatory $CD4^+$ T cell subpopulations (Fig. 1). Consequently, it ameliorates the suboptimal healthy status of the model mice. These initial findings offer valuable insights into the potential clinical implications of immunometabolic regulatory networks driven by polysaccharides.

2. Materials and methods

2.1 Chemicals and regents

The *D. officinale* stem was obtained from Zhejiang Senyu Co., Ltd. (Zhejiang, China). It was dried in a hot air oven at 60 ℃ for 120 min to remove moisture. After drying, the stem was pulverized into ultrafine powder and screened through a 40-mesh sieve to obtain a uniform particle size. The DEAE-52 cellulose and Sephadex G-100 used in the study were purchased from Shanghai Yuanye Biological Technology Co., Ltd. (Shanghai, China).

Analytical-grade chemicals and reagents were used in all other experiments. Hematoxylin and eosin (H&E) and periodic acid-Schiff (PAS) were obtained from Shanghai Yuanye Biological Technology Co., Ltd. (Shanghai, China). The Occludin, Zonula occludens 1 (ZO-1), IL-10, IL-22, IL-17A, and *β*-actin were purchased from Wuhan Sanying (Wuhan, China). The CD4 antibody was purchased from HuaBio (Hangzhou, China). The forkhead box protein 3 (Foxp3) antibody was purchased from Zenbio (Chengdu, China). The retinoic acid receptor-related orphan receptor γt (RORγt) antibody was purchased from Bioss (Beijing, China). The horseradish peroxidase (HRP) conjugated goat anti-rabbit IgG (H + L), the DyLight550 Conjugated AffiniPure goat anti-rabbit IgG (H + L), the 4′,6-diamidino-2-phenylindole (DAPI), and the FITC Conjugated AffiniPure goat anti-rabbit IgG (H + L) were purchased from Boster Biological Technology Co., Ltd. (Wuhan, China). The BCA protein concentration assay kit was purchased from the Beyotime Institute of Biotechnology (Nantong, China). The DAB immunohistochemistry (IHC) color development kit and the PAGE gel fast preparation kit was purchased from Shanghai EpiZyme Biotechnology Co., Ltd. (Shanghai, China). The IgA and IgM enzyme-linked immunosorbent assay (ELISA) kits were purchased from Multi sciences (Hangzhou, China). Complement C3c Fs and complement C4 Fs were purchased from DiaSys Diagnostic Systems GmbH. Affinity Biosciences (Shanghai, China).

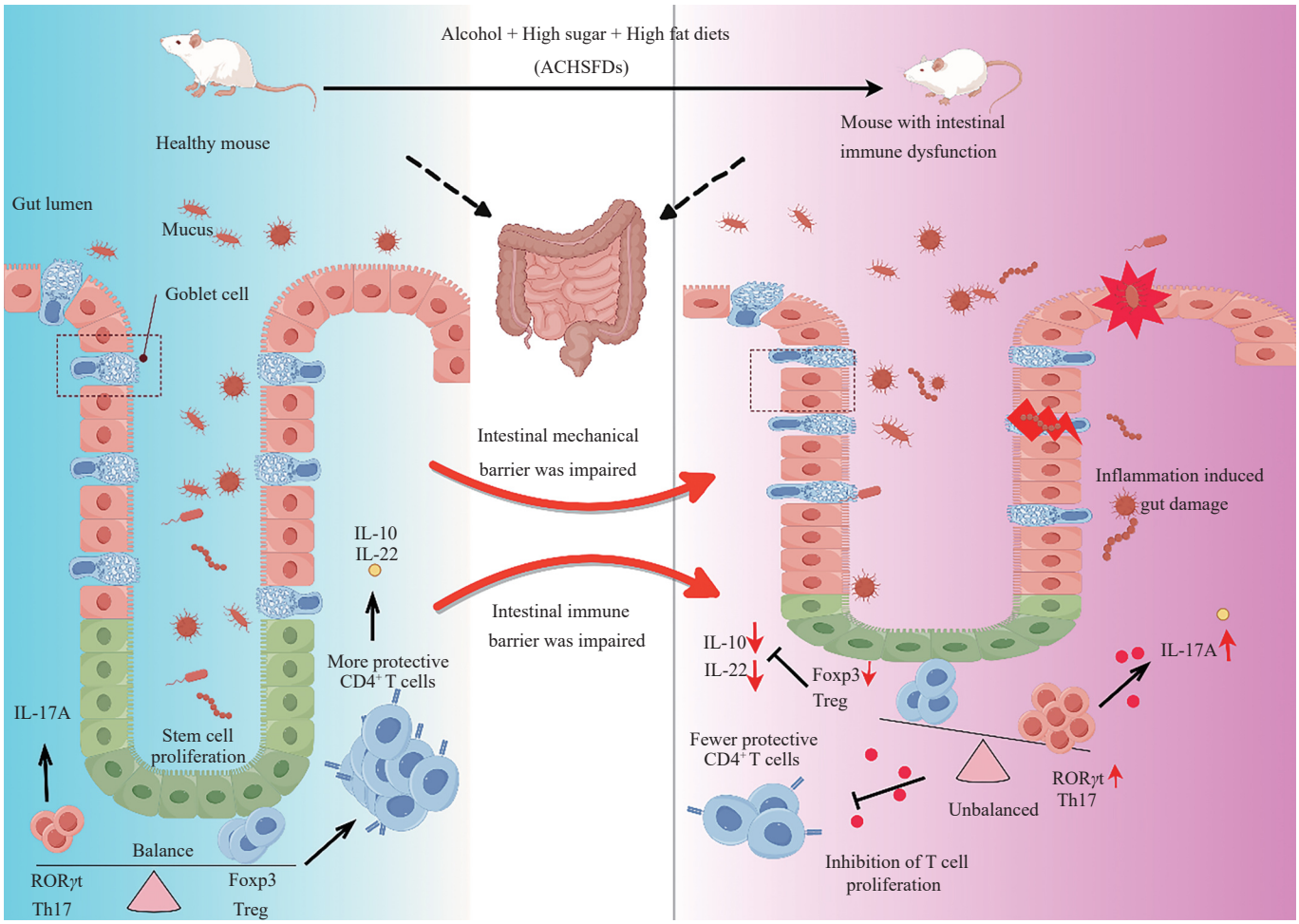

Fig. 1 Map of the mechanism of gut $CD4^+$-Th17/Treg immune imbalance models.

2.2 *Extraction, isolation, and purification of crude polysaccharide*

The DOPS (yield 27.14%) were obtained from *D. officinale* were first extracted by refluxing the dried powder twice with purified water (1:20, *m/V*) at 100 ℃ for 1.5 h each time. The resulting extraction liquids were then vacuum filtered to retain the supernatant, combined, and concentrated to a volume of 50 mL. Next, the concentrated solution was slowly added to four times its volume of anhydrous ethanol and left at 4 ℃ overnight for precipitation. Afterwards, the floccule was subjected to centrifugation at 4 000 × *g* for 20 min to remove the supernatant, and then lyophilized using freeze-drying. Moreover, the crude polysaccharides were subjected to Sevag deproteinization using an apparatus to purify them, resulting in the isolation of the DOPS[21].

To purify DOPS further, it was redissolved in high-purity water, filtered through a 0.45 μm membrane, and then subjected to purification using DEAE-52 cellulose (45 mm × 200 mm). The purification process involved sequential elution of the column with distilled water followed by NaCl solutions of different concentrations (0.10 and 0.50 mol/L) at a flow rate of 1 mL/min. Each fraction (10 mL per tube) was monitored at 488 nm using the phenol-sulfuric acid method. The dialysis and lyophilization were performed on each fraction for additional purification. The dried polysaccharides from each fraction were redissolved in high-purity water to a concentration of 5.0%. These polysaccharide solutions (5 mL) were then loaded into a Sephadex G-100 column (30 mm × 320 mm) and eluted with high-purity water at a flow rate of 10 mL/h. The eluted fractions (5 mL per tube) were collected, concentrated, and lyophilized to obtain the DOPS100.

2.3 *Structural characterization of polysaccharides*

2.3.1 *Physicochemical properties of DOPS and DOPS100*

The contents of two polysaccharides from *D. officinale* were determined using various methods. The total polysaccharides, total glucuronic acid, total flavone, total saponin, and total phenol contents were measured by phenol sulfuric acid, *m*-hydroxybiphenyl, $NaNO_2$-$Al(NO_3)_3$-NaOH colorimetric, vanillin-perchloric acid colorimetric method, and Folin-Ciocalteu reagent methods, respectively[22].

2.3.2 *Fourier transform infrared spectroscopy (FT-IR) analysis and congo red test*

The DOPS/DOPS100 (2 mg) as ground with 100 mg KBr powder and pressed into pellets for FTIR determination in the range of 4 000–400 cm^{-1} (Nicolet Co., USA). For the congo red test, the DOPS/DOPS100 solutions (1 mg/mL, 2 mL) were mixed well with congo red solution (80 mmol/L, 2 mL). NaOH solution of 1 mol/L was added dropwise to the mixed solution to achieve NaOH

concentrations of 0, 0.10, 0.20, 0.30, 0.40, and 0.50 mol/L respectively. The visible spectrum was scanned at 400−800 nm using a ultraviolet-visible (UV-Vis) spectrophotometer, and the maximum absorption wavelength was recorded. A blank control was conducted using congo red solution after rinsing with distilled water.

2.3.3 Monosaccharide composition analysis of DOPS and DOPS100

The monosaccharide composition was determined using a previous precolumn derivatization high performance liquid chromatography (HPLC) method[23-24]. The hydrolysis of DOPS or DOPS100 acid hydrolysis solution was performed by adding 0.50 mol/L 1-phenyl-3-methyl-5-pyrazolone (PMP) methanol solution and heating it at 70 ℃ for 90 min. Then, the hydrochloric acid solution was added and mixed. Afterward, trichloromethane was extracted thrice and centrifuged at 12 000 × *g* for 20 min to isolate the supernatant. The resulting derivative supernatant was subjected to HPLC analysis using an Agilent Co. HPLC system with Welch Ultimate XDB C_{18} (4.6 mm × 250 mm, 5 μm, Agilent, USA) column and an ultraviolet detector at 250 nm. The HPLC analysis conditions were as follows: column temperature, 30 ℃; mobile phase, 0.01% phosphate buffer and acetonitrile; flow rate, 1.0 mL/min.

2.3.4 Molecular morphological analysis

The morphology of samples was observed through a field emission scanning electron microscope (FE-SEM, HITACHI Regulus 8100, Japan) at an acceleration voltage of 20 kV. And the related elemental distribution was analyzed with energy-dispersive X-ray spectroscopy (EDS, Oxford Ultim Max 65, UK).

2.4 Animal experimental design

ICR male mice were obtained from the SLAC ANIMAL (Shanghai) Experimental Animal Center Co., Ltd. (SCXK (Hu) 2022-0004). The mice were adaptively given food and water for 3 days and maintained at a constant room temperature of (22 ± 2) ℃ and a humidity of 50%−70% for 12 h light/dark cycles. All experiments were performed in compliance with the Regulation of Experiment Animal Administration issued by the Ministry of Science and Technology of the People's Republic of China. The experiment received approval from the Ethics Committee of Zhejiang University of Technology (MG20220923012). To better simulate the adverse lifestyle of ACHSFDs in humans, this study randomly divided all male ICR mice into 4 groups (n = 10): normal group (NG), model group (MG), DOPS group (100 mg/kg), and DOPS100 group (100 mg/kg). The sub-healthy mice were induced by ACHSFDs.

After 7 weeks of modeling, the drug was administered. The normal group was given the same volume of distilled water (10 mL/kg), while the remaining drug were administered in equal amounts once a day for 5 weeks. The blood was collected through the eye sockets, spleen, thymus, colon, and ileum tissues were collected and stored in a refrigerator at −80 ℃. To view the comprehensive experimental technical route, refer to Fig. 2 for the flowchart.

2.4.1 ACHSFDs diet design

ACHSFDs consisted of a high sugar and fat diet (Trophic Animal Feed High-Tech Co., Ltd., Nantong, China, TP0800, 20% sucrose, 15% lard, 1.20% cholesterol, 0.20% sodium cholate, an appropriate amount of casein, dicalcium phosphate, and stone powder, etc.) and ethanol. The model group were given 4% ethanol for 4 consecutive days, which was increased to 8% on the 6th day and then increased by 4% every 3 days until reaching 50%.

2.4.2 General signs and behavior tests

The weight of mice was recorded once every 2 weeks during the experiment. The back of mice was photographed using a thermal imaging camera, and the back temperature was measured using FLIR ONE software. In the last day of the experiment, the holding power of the mice was recorded. Additionally, autonomous activity tests were conducted in the last week of the experiment. Thirty min after administration, the mice from each group were placed into a multifunctional mouse automatic activity recorder to acclimate for 2 min. The locomotion activity of each mouse was then measured and collected within 5 min.

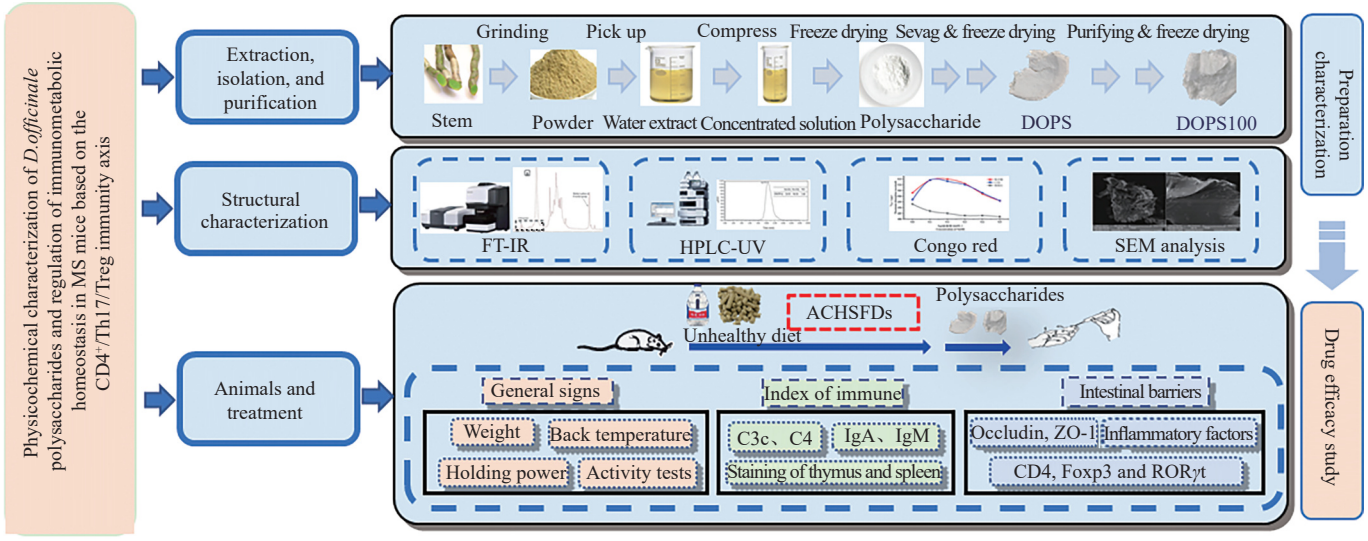

Fig. 2 Flow chart of experimental technical route.

2.4.3 Measurement of serum immunoglobulin and serum complement

Mice were fasted overnight after undergoing a 5-week treatment. Blood was then drawn from the ophthalmic venous plexus and centrifuged at 3 500 r/min for 10 min to collect the serum. The collected serum was used for detecting levels of serum complement C3c and C4 using corresponding kits on a Hitachi 7060 Automatic Biochemical Analyzer (Hitachi, Shanghai, China). Additionally, levels of IgA and IgM in the serum were measured using ELISA kits, following the instructions of manufacturer.

2.4.4 Histopathology assessment of immune organ

Tissues (gut, spleen, and thymus) were collected from each mouse, and gross lesions were recorded. The collected tissues were then fixed with a 4% formalin solution, dehydrated using different concentrations of alcohol, and embedded in paraffin. Subsequently, 4 μm paraffin sections were prepared from the embedded tissues. Finally, the histopathological examination of the tissue was assessed using H&E staining, PAS staining. Briefly, the tissues of gut, spleen and thymus were stained with H&E. The gut tissues were stained with PAS and the nuclei were counterstained with hematoxylin. All H&E and PAS staining were photographed with the biological microscope (BX43, Olympus, Japan) and analysed with the Image-Pro Plus software.

Intestinal mucosal damage was evaluated using the improved Chiu's score[25]: grade 0, normal mucosa; grade 1, development of subepithelial Gruenhagen's space at the tip of the villus; grade 2, extension of the space with moderate epithelial lifting; grade 3, massive epithelial lifting with a few denuded villi; grade 4, denuded villi with dilated capillaries; and grade 5, disintegration of the lamina propria, ulceration, and hemorrhage. Higher scores were interpreted to indicate more severe damage.

2.4.5 IHC and immunofluorescence (IF) analysis

The expression of Foxp3 and RORγt proteins in the gut tissue was evaluated using immunohistochemical staining. The paraffin tissue sections were incubated with Foxp3 and RORγt antibodies, followed by incubation with a secondary antibody, goat anti-rabbit IgG. The signals were then observed using DAB solution, and the nuclei were counterstained with hematoxylin. Under the microscope, positive expression appeared as a yellow color. The protein levels were quantified by measuring the integrated option density (IOD) within the positive area.

Similarly, the expression of IL-10, CD4, Occludin, and ZO-1 proteins in the gut tissue were evaluated using IF staining. The paraffin tissue sections were incubated with IL-10, CD4, Occludin, and ZO-1 antibodies, followed by incubation with either the fluorescein isothiocyanate (FITC) Conjugated AffiniPure Goat Anti-Rabbit IgG (H + L) or the DyLight550 Conjugated AffiniPure Goat Anti-rabbit IgG (H + L) under dark conditions. The nuclei were counterstained with DAPI staining solution. Under the microscope, positive expression appeared as green or red color.

2.4.6 Western blot analysis

The protein concentration of the intestinal protein, extracted with radio immunoprecipitation (RIPA) buffer, was determined using the BCA protein assay kit. A total protein amount of 80 μg was loaded onto a gel and separated through gel electrophoresis. Subsequently, the proteins were transferred to a polyvinylidene fluoride (PVDF) membrane and incubated with the primary antibody overnight at 4 °C. Following a wash with tris buffered saline with Tween-20 (TBST), the target proteins were incubated with the horseradish peroxidase-conjugated secondary antibody IgG (1:5 000). The expression of CD4 protein was detected utilizing the Western blotting technique. Finally, the results were visualized through the enhanced chemiluminescence (ECL) Western blotting detection system. The expression level of the target proteins was normalized against the control β-actin.

2.5 Statistical analysis

Results were statistically evaluated using SPSS Statistics 19.0. Significant group differences were determined by Spearman correlation tests (Student's *t*-test, $P < 0.05$, |correlation coefficient| > 0.30). Statistically significant was set as $P < 0.05$. Graphs were created using GraphPad Prism 8.0.

3. Results

3.1 Properties of DOPS and DOPS100

3.1.1 Chemical composition

To estimate the main polysaccharide components of DOPS and DOPS100, a suite of chemical and spectral tools were used. The study revealed that DOPS-1 (neutral polysaccharides) accounted for the main components of DOPS during the purification process (Fig. 3A). Furthermore, the total glucuronic content of DOPS100 (Fig. 3B) was significantly lower ((0.37 ± 0.05)%) compared to DOPS ((1.15 ± 0.18)%). Similarly, the total flavonoid contents of the purified polysaccharides were significantly reduced compared to DOPS ((0.36 ± 0.03)% *vs*. (0.52 ± 0.05)%, respectively; $P < 0.05$). Moreover, both polysaccharides were almost devoid of total saponins and total phenolic components.

3.1.2 Monosaccharide composition

The HPLC method of precolumn derivatization with PMP was used to determine the monosaccharide composition of DOPS and DOPS100. It can be seen that DOPS and DOPS100 are heteropolysaccharides composed of mannose, glucose, and arabinose (Fig. 3C). The molar ratio of these monosaccharide components in DOPS is 6.00:1.00:0.05, and in DOPS100 it is 11.65:1.00:3.26.

3.1.3 Analysis of functional groups

FT-IR spectroscopy in the range of 4 000−400 cm^{-1} was used for the characteristic absorption analysis. The FT-IR spectra of DOPS and DOPS100 are similar and exhibit various typical absorption bands of polysaccharides (Fig. 3D). The broad and strong absorption band observed at 3 366 cm^{-1} in the 3 500−3 100 cm^{-1} region can be attributed to the stretching vibration of the polysaccharide hydroxyl group (−OH) involved in hydrogen bonding. The absorption at 2 922 cm^{-1} in the 3 000−2 800 cm^{-1} region corresponds to the C−H stretching vibration of

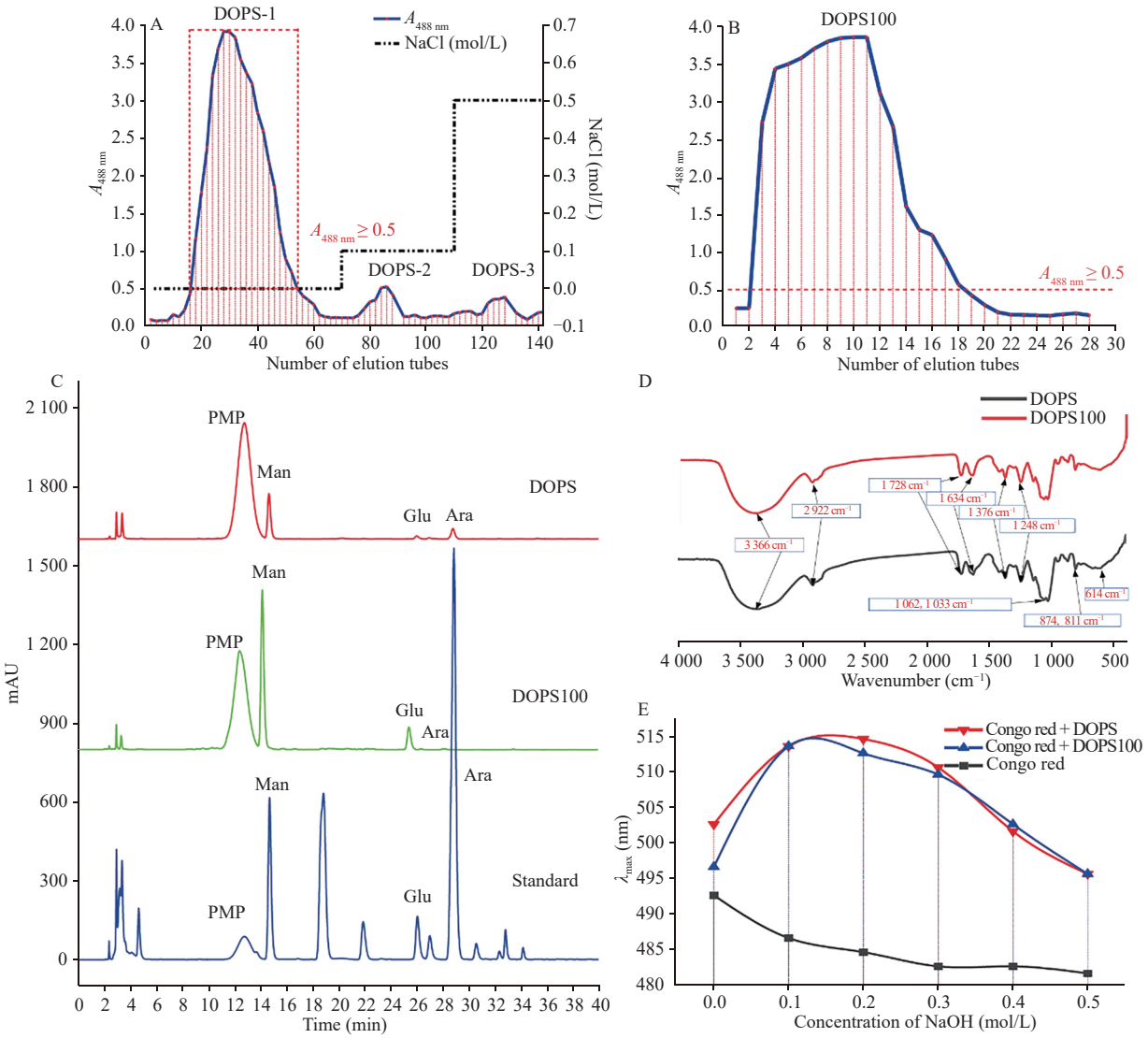

Fig. 3 Schematic diagram of the purification and structural characterization results of *D. officinale* polysaccharides. (A) Elution profile of polysaccharides on DEAE-52 cellulose; (B) Elution profile of polysaccharides on Sephadex G-100; (C) Monosaccharide composition analysis by HPLC; (D) FT-IR spectra; (E) The determination of the chain conformation of polysaccharides.

the methylene group, which the bond at 1 728 cm^{-1} is assigned to the valence vibration of C=O. The peak at 1 634 cm^{-1} indicates the stretching vibration of the free carboxyl group[26]. The C−H stretching vibration of the methyl group is observed at 1 376 cm^{-1}, and the peaks near 1 248 cm^{-1} are attributed to the symmetric C−H bending vibration of the methyl group and the C−O vibration of the *O*-acetyl group, respectively[27]. The presence of pyranose form in the polysaccharides is indicated by the absorption at 1 062 and 1 033 cm^{-1}[28]. The presence of *β-D*-mannopyranose is revealed by the absorption peak at 874 cm^{-1}, and the absorption peak at 614 cm^{-1} indicates the presence of pyranose glucose ring in the polysaccharide[29].

3.1.4 Degree of esterification

The absorption peaks at around 1 728 and 1 634 cm^{-1} indicate the C=O stretching vibration of esterified carboxylic groups (COO−*R*) and the asymmetric stretching of carboxylate anions (COO−), respectively[30-31]. The esterification levels of DOPS and DOPS100 were assessed by analyzing the ratio of the peak area at 1 728 cm^{-1} over the sum of the peak areas of 1 728 and 1 634 cm^{-1}[32].

The degree of esterification was analyzed and it was found to be 50.46% for DOPS and 50.03% for DOPS100 (Fig. 3D). Previous studies have shown that the degree of esterification of polysaccharides influences their immunomodulatory activity[33-34].

3.1.5 Spatial conformation

The chain conformation of polysaccharides in solution has a significant impact on their biological activities. Triple-helical structures of *β*-glucans have been found to exhibit enhanced biological activity[33-35].

To investigate the structure of the polysaccharides, the composite solution of the polysaccharide and congo red was subjected to a congo red test[36]. The λ_{max} values of congo red + DOPS and congo red + DOPS100 were observed to be sequentially red-shifted and blue-shifted (Fig. 3E), suggesting that the presence of triple-helical conformations in both polysaccharides[37].

3.1.6 Molecular morphology

SEM was applied in the study to observe the surface morphology of DOPS and DOPS100. The results revealed that a loose filamentous crosslink with cobweb fragments can be seen in DOPS, and the DOPS100 surface is smoother and exhibits fewer pores and cracks in its cross-section compared to DOPS (Figs. 4A-C, a-c). Additionally, white spots were observed on the surface. On the other hand, DOPS exhibited an irregular granular shape with internal small holes, which could possibly be attributed to the aggregation of polysaccharide molecules. The EDS spectrum (Figs. 4D, d, E, e) further supported these findings by showing that DOPS100 mainly consisted of carbon and oxygen. Based on these observations, it can be deduced that DOPS100 was successfully purified[38].

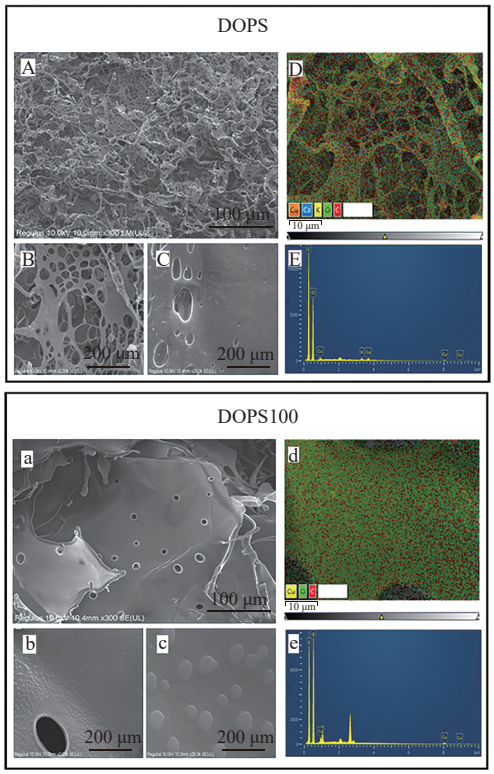

Fig. 4 Representative SEM images and EDS of DOPS and DOPS100. (A, a) 300×, (B, b) 1 000×; (C, c) 2 000×; (D, d) Scan imagery of EDS; (E, e) Maps of the distribution of elements spectrum curves.

3.2 Animals experiments

3.2.1 Effects of DOPS and DOPS100 on general signs and behavior in sub-health mice

Indications pertaining to the physical realm hold the potential to unveil the comprehensive state of an organism. For instance, variations in body weight offer glimpses into the intricate balance of caloric equilibrium maintained over the course of time. Grip and vertigo time are measures that quantitatively assess symptoms like fatigue and dizziness. Compared with the normal group, the model group showed significant decreases in trends of body weight and holding power after 12 weeks of modeling ($P < 0.01$) (Figs. 5A, B), as well as significant increases in dizziness time and back temperature ($P < 0.01$) (Figs. 5C-E). Compared with the model group, the DOPS100 riser the trends of body weight (Fig. 5A), both DOPS and DOPS100 significant increases holding power of the sub-healthy mice after 5 weeks of administration (Fig. 5B). More and more, both DOPS and DOPS100 significant decreases in back temperature and dizziness time ($P < 0.01, 0.05$) (Figs. 5C-E).

The effects of DOPS and DOPS100 on anxiety and exploratory behaviors in sub-healthy mice was evaluated using the autonomous activity experiment. Locomotive movements of mice in the model group were significantly reduced compared to the normal group ($P < 0.05$) (Figs. 5F-H), and the time spent not moving was significantly higher ($P < 0.05$) (Fig. 5I). Comparison with the model group, the DOPS group exhibited significantly higher movement speed and distance ($P < 0.05$) (Figs. 5G, H), and the immobility time of DOPS and DOPS100 groups was notably decreased ($P < 0.05$) (Fig. 5I). The polysaccharides-intervened (DOPS and DOPS100) groups exhibited an excellent healthy function on the above-mentioned changes, implying that polysaccharides have benefits on the mental changes caused by sub-healthy.

3.2.2 Effects of DOPS and DOPS100 on immune organ in sub-healthy mice

Thymus and spleen play an important role in immunoregulation, and their indexes serve as significant indicators of immune function. Compared with the normal group, the spleen index significantly increased ($P < 0.01$) (Fig. 6C), and the thymus index of the model group tended to increase by 16.82% (Fig. 6D). H&E staining of the thymus and spleen revealed that the thymic lobules of the model group showed indistinct structural characteristics, including an indistinct boundary between the

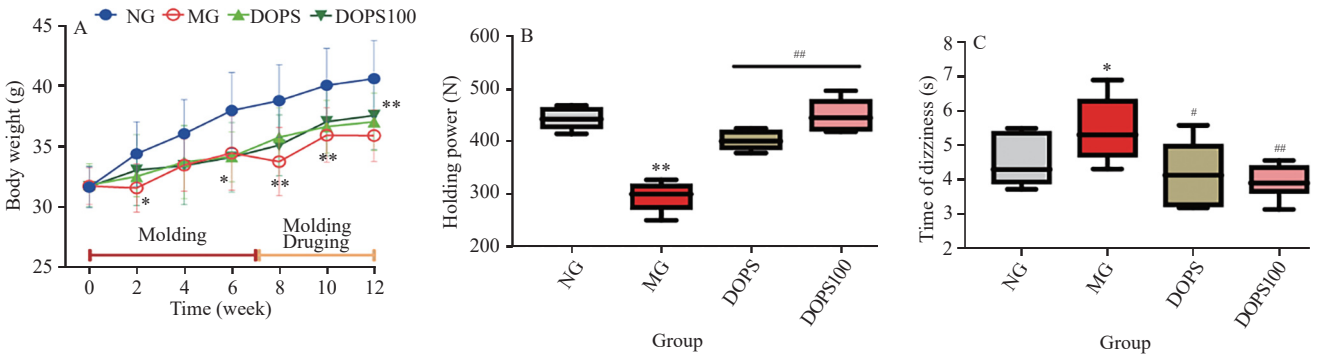

Fig. 5 Effects of DOPS and DOPS100 on general signs and behavior in sub-healthy mice. (A) The tendency chart of body weight; (B) Holding power; (C) Time of dizziness; (D) The heat map of back temperature; (E) The infrared thermography of back temperature; (F) Open field test; (G) Movement speed; (H) Movement distance; (I) Immobility time. Compared with the NG $^{*}P < 0.05$, $^{**}P < 0.01$; compared with the MG $^{\#}P < 0.05$, $^{\#\#}P < 0.01$.

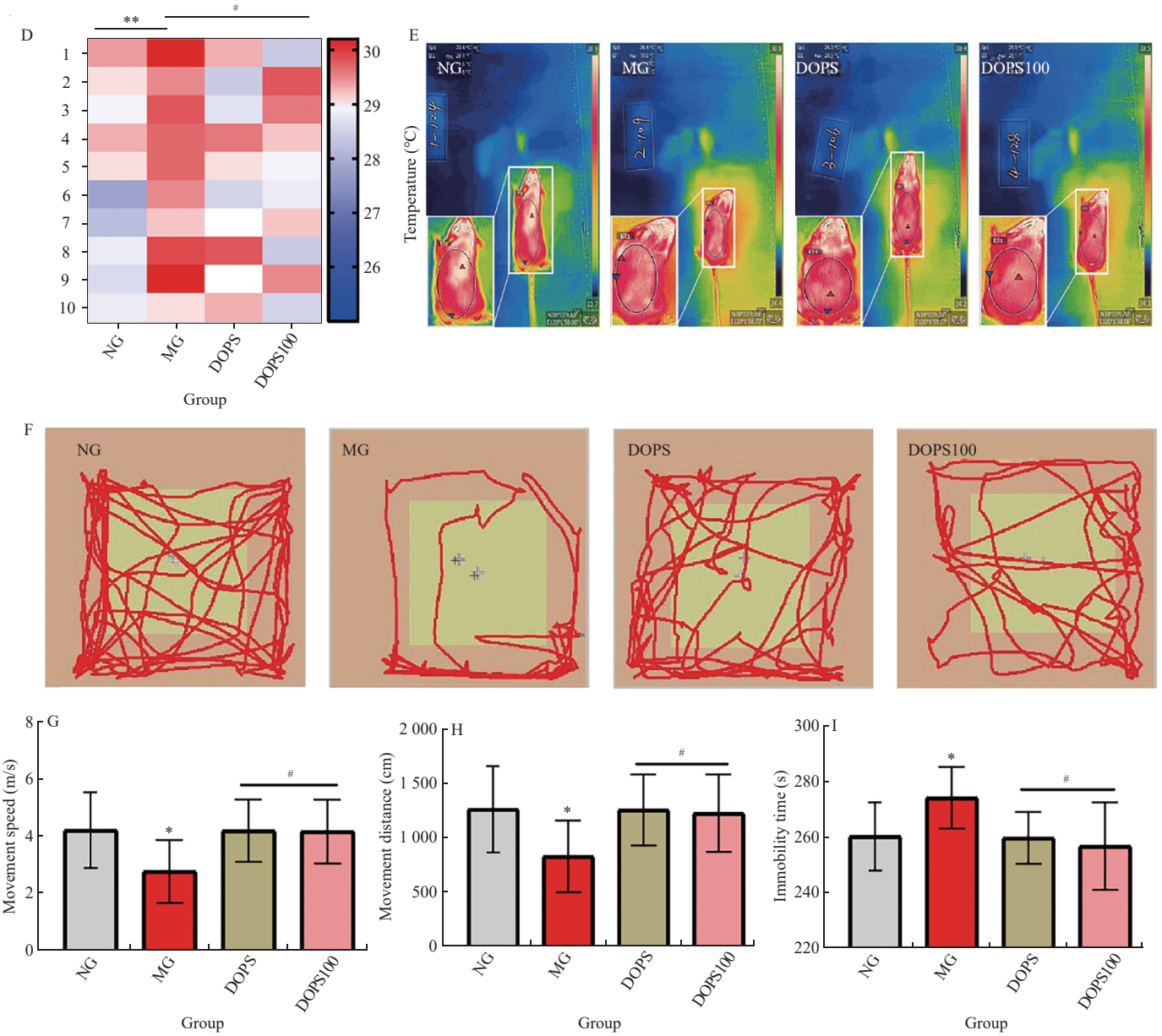

Fig. 5 (*Continued*)

cortex and medulla, and an enlarged medullary region. Similarly, the splenic tissues of the model group exhibited scattered white medullary structure and germinal centers, along with a reduced number of lymphocytes (Figs. 6A, B). These findings suggest that long-term unhealthy diet habits lead to immune organ damage in model group.

After 5 weeks of drug administration, the spleen index significantly reduced in the DOPS100 group ($P < 0.05$) (Fig. 6C), and there was also a tendency to reduce the thymus index by 10.61% (Fig. 6D). There were tendency to reduce the spleen index and the thymus index in DOPS group. H&E staining showed that the intervention of DOPS and DOPS100 improved the thymus tissue structure in model group, leading to normalized thymus lobules and a clear demarcation of the cortex and medulla. The medullary area was significantly reduced. Additionally, the spleen peritoneum of the model group tended to be complete, resulting in a significant increase in the white medulla area and a convergence of the germinal center. These observations indicated a better restoration of the splenic tissue morphology (Figs. 6A, B). In conclusion, DOPS and DOPS100 could improve immune organ injury in sub-healthy mice.

3.2.3 Effects of DOPS and DOPS100 on serum immune indices in sub-healthy mice

Serum immunoglobulin and complement play crucial roles in the humoral immune response. The results demonstrated that compared to the normal group, serum levels of IgA and IgM in the model group significantly decreased ($P < 0.05$) (Figs. 6E, F), and levels of complement C3c and C4 significantly increased ($P < 0.01$) (Figs. 6G, H) in model group. Following 5 weeks of administration, compared with the model group, DOPS and DOPS100 significantly increased serum levels of IgA and IgM levels ($P < 0.01$, 0.05) (Figs. 6E, F), while significantly decreasing the complement C4 level ($P < 0.05$) (Fig. 6H). Moreover, DOPS100 significantly reduced the complement C3c level ($P < 0.05$),

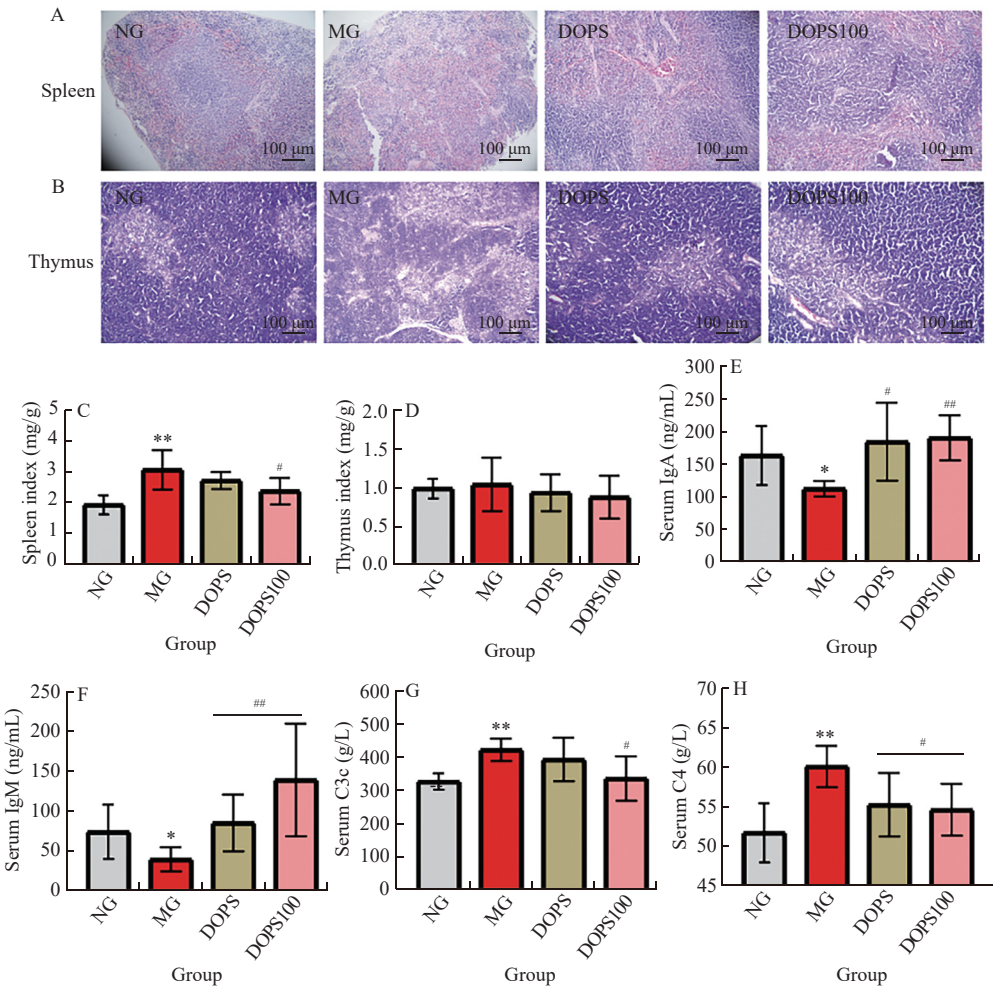

Fig. 6 Effects of DOPS and DOPS100 on serum immune indices and immune organ in sub-healthy mice. (A-B) Representative graph (200×) of H&E staining of the spleen and the thymus, respectively (scale bar = 100 μm); (C-D) The indexes of the spleen and thymus, respectively; (E) Serum IgA; (F) Serum IgM; (G) Serum complement C3c; (H) Serum complement C4. Compared with the NG $^{*}P < 0.05$, $^{**}P < 0.01$; compared with the MG $^{\#}P < 0.05$, $^{\#\#}P < 0.01$.

and there was a trend of reducing the complement C3c level in the DOPS group (Fig. 6G). The discoveries suggested that both DOPS and DOPS100 to modulate the levels of serum immune factors and complement to improve the humoral immune function.

3.2.4 Effects of DOPS and DOPS100 on reshaping intestinal mechanical barriers in sub-healthy mice

Intestinal mechanical and immune barriers maintain intestinal health by preventing pathogenic microorganisms and toxins from entering the body through the synergistic formation of an intestinal barrier by physical structure and immune function. H&E staining of intestinal tissues showed that in the normal group, the villi were neatly arranged and of moderate length, and the ileal epithelial cells were structurally intacted and arranged in phase (Fig. 7A). However, in the model group after 12 weeks of modeling, the length of villi was significantly shorter and the depth of crypt was significantly increased ($P < 0.01$) (Figs. 7B, C). Additionally, the ratio of villous height/crypt depth (VH/CD) was significantly lower ($P < 0.01$) (Fig. 7D), and the pathological score of intestinal tissue was significantly increased ($P < 0.01$) (Fig. 7E). The expression levers of tight junction proteins, including Occludin (Figs. 7F, G) and ZO-1 (Figs. 7L, M), were assessed through IF analysis and found to be significantly reduced ($P < 0.01$, 0.05) (Figs. 7F-M). These findings suggest that long-term "ACHSFDs" can cause damage to the tight junctions of the colon and disrupt the intestinal mechanical barrier function, resulting in the translocation of intestinal pathogenic bacteria into the bloodstream.

Compared with the model group, after 5 weeks of drug administration, DOPS significantly decreased the pathological score of intestines ($P < 0.01$) and significantly increased the VH/CD ratio ($P < 0.01$). In particular, DOPS100 not only significantly improved the aforementioned indicators but also significantly reduced the depth of crypt ($P < 0.05$) (Figs. 7A-E). The results demonstrated a significant increase in Occludin expression in ileum tissue following treatment with DOPS100 ($P < 0.01$). Additionally, the expression level of ZO-1 was found to be significantly elevated in both colon and ileum tissue ($P < 0.01$) when compared to the model group (Figs. 7H-K). Moreover, DOPS significantly increased the expression levels of ZO-1 in both mouse ileum and colon tissue ($P < 0.01$, 0.05) (Figs. 7J, K). It suggested that DOPS and DOPS100 could improve the pathological and physiological state of the intestine, regulate the expression of intestinal tight junction proteins, and enhanced the intestinal mechanical barrier in sub-healthy status.

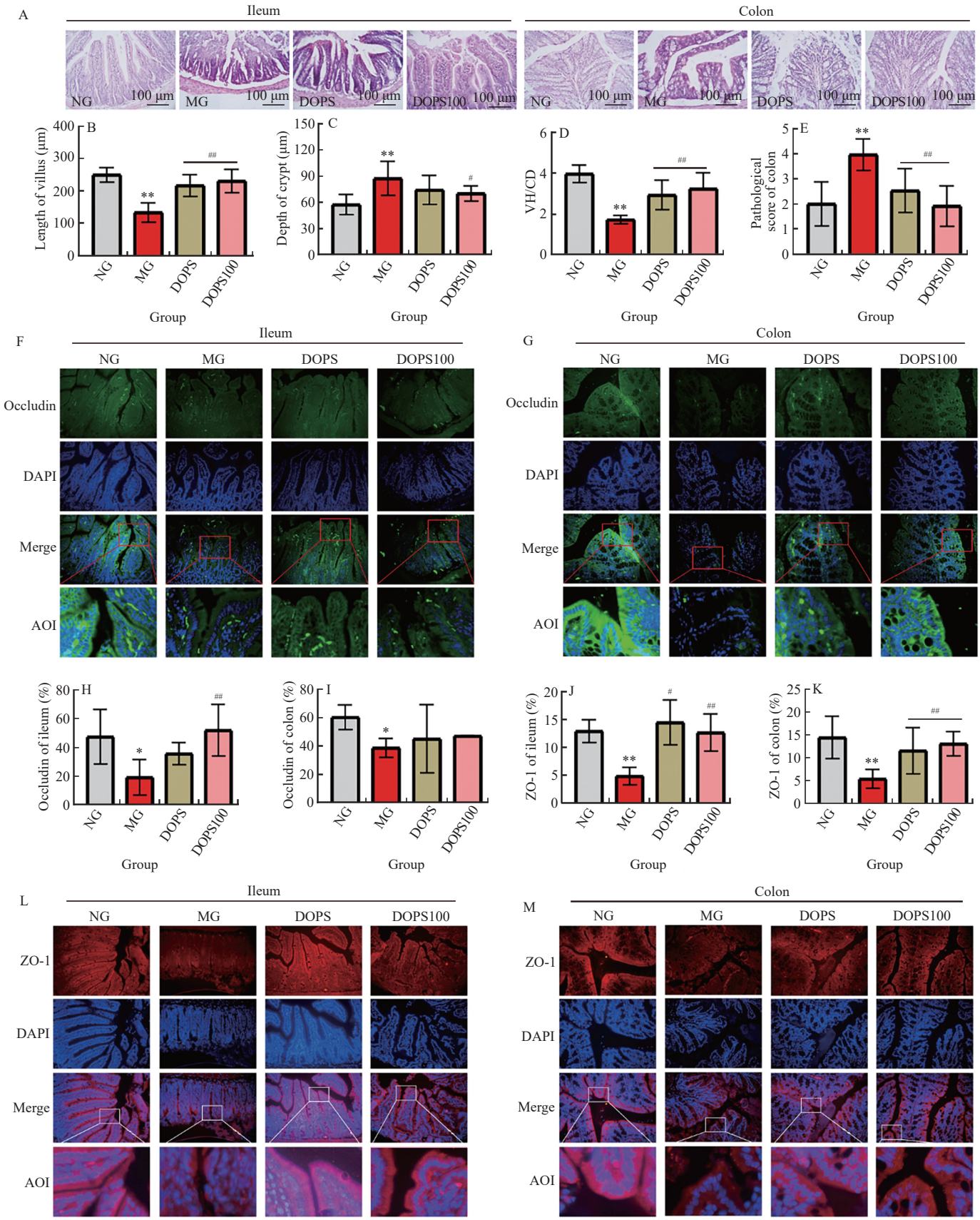

Fig. 7 Effects of DOPS and DOPS100 on reshaping intestinal mechanical barriers in sub-healthy mice. (A) Representative graph (400×) of H&E staining of the ileum and the colon, scale bar = 100 μm; (B) The length of villi; (C) The depth of crypt; (D) The ratio of VH/CD; (E) The pathological score of colon; (F-G) The IF of Occludin (400×), scale bar = 100 μm; (H-I) Occludin of ileum and colon; (J-K) ZO-1 of ileum and colon; (L-M) The IF of ZO-1 (400×), scale bar = 100 μm. Compared with the NG $^{*}P < 0.05$, $^{**}P < 0.01$; compared with the MG $^{\#}P < 0.05$, $^{\#\#}P < 0.01$.

3.2.5 *Effects of DOPS and DOPS100 on reshaping intestinal immune barriers in sub-healthy mice*

Alkaline phosphatase staining is used to observe changes in the intestinal alkaline phosphatase (IAP) levels. The study found that after 12 weeks of modeling, the expression of IAP in colon and ileum in the model group was significantly reduced ($P < 0.01$) compared with the normal group (Figs. 8A-C). Alcian blue (AB) and PAS (Figs. 8D, G) staining of intestinal tissues (ileum and colon) further showed that the glands and intraepithelial goblet cells in the normal group were normal and tightly arranged, with a flat mucosal surface. However, in the model group, the glands were ruptured abnormally, and some of the intraepithelial goblet cells were disorganized and sparsely arranged. There were significantly decreased in both goblet cells and mucus secretion (Figs. 8E, F, H, I) in the model group after 12 weeks of modeling compared with that in the normal group ($P < 0.05$).

Compared with the model group, after 5 weeks of administration, both DOPS and DOPS100 could significantly enhance the expression level of IAP ($P < 0.01$) (Figs. 8A-C). Further AB and PAS staining showed that after treatment with DOPS and DOPS100, there was a discernible improvement in both the abundance of intestinal epithelial goblet cells and the structural integrity of tissue glands, albeit to varying degrees (Figs. 8D-I). The results show that DOPS and DOPS100 could improve the intestinal immune barriers in sub-healthy mice.

3.2.6 *Effects of DOPS and DOPS100 on reshaping the $CD4^+$-Th17/Treg pathway in sub-healthy mice*

The balance of intestinal $CD4^+$-Th17/Treg is essential for the regulation of autoimmune response and metabolic disorders. Foxp3 and RORγt, which are nuclear transcription factors of Treg and Th17 respectively. Western blot showed that the expression level of Foxp3 protein in the colon of model group was significantly reduced ($P < 0.05$) (Figs. 9A, D). Additionally, the expression level of CD4 protein exhibited a declining pattern (Figs. 9A, C). This phenomenon was also confirmed by IF or IHC staining (Figs. 9E, F). And the expression level of RORγt protein was significantly increased in the model group ($P < 0.01$) (Figs. 9A, B). These findings suggest that the long-term poor diet of "ACHSFDs" may cause abnormalities in intestinal $CD4^+$ T-cell and Th17/Treg immune balance.

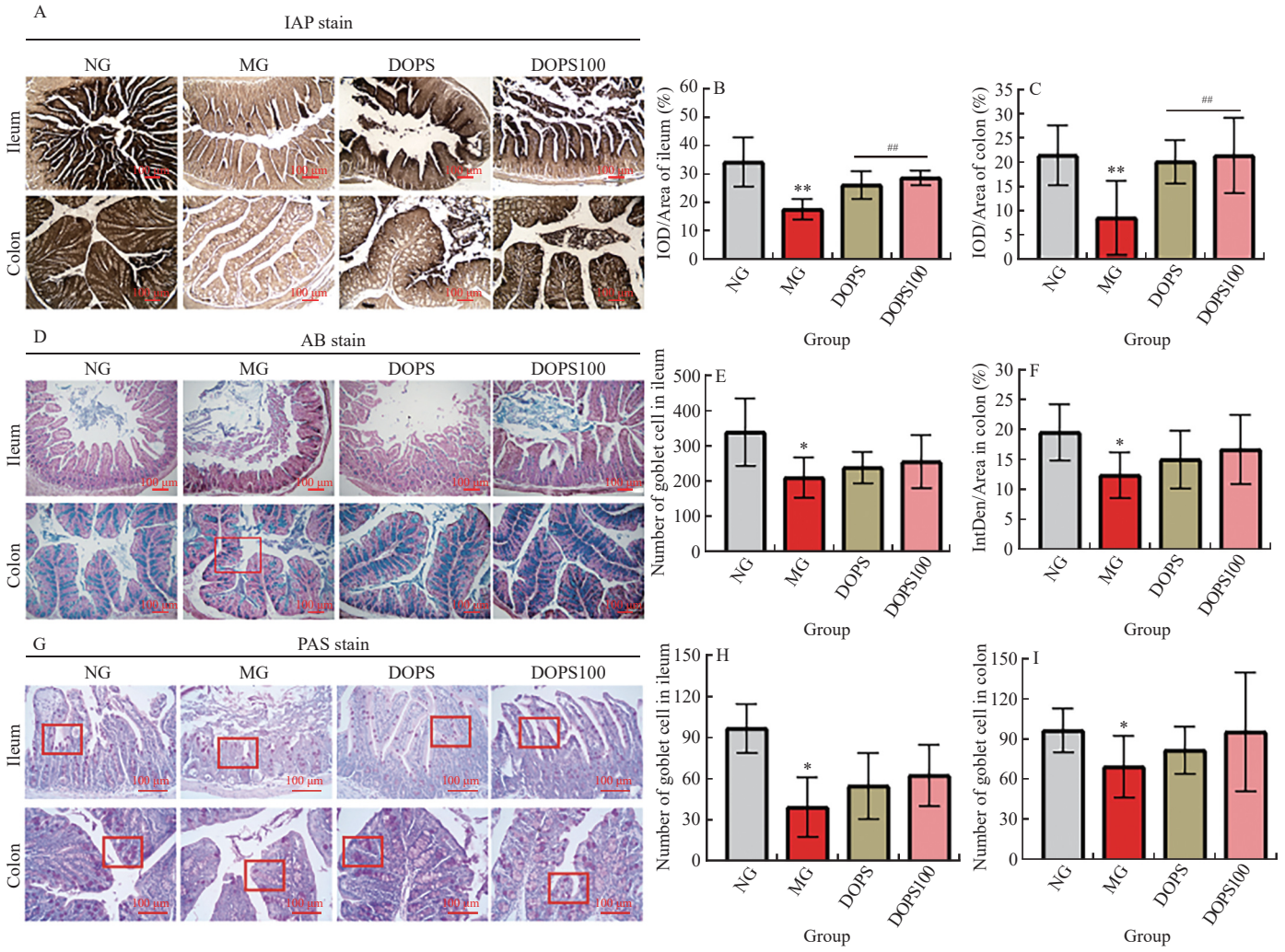

Fig. 8 Effects of DOPS and DOPS100 on reshaping intestinal immune barriers in sub-healthy mice. (A-C) IAP representative images of colon and ileum (200×), scale bar = 100 μm and statistical charts of colon; (D, E) AB representative images of colon and ileum (200×), scale bar = 100 μm and statistical charts of the number of intraepithelial goblet cells in the ileum; (F) Expression of colonic acidic mucin; (G-I) PAS representative images of colon and ileum (400×), scale bar = 100 μm and statistical charts of the number of intraepithelial goblet cells. Compared with the NG $^*P < 0.05$, $^{**}P < 0.01$; compared with the MG $^{\#\#}P < 0.01$.

After 5 weeks of drug administration, compared with the model group, DOPS and DOPS100 could significantly increase the expression of CD4 protein in colon ($P < 0.01$, 0.05) (Figs. 9A, C). The protein expression of Foxp3 was significantly increased ($P < 0.01$) (Figs. 9A, D). The expression of RORγt protein was significantly decreased ($P < 0.01$, 0.05) (Figs. 9A, B). Similar results were found by IF and IHC of CD4, Foxp3, and RORγt in intestine (Figs. 9E-G). These results suggested that DOPS and DOPS100 may remodel intestinal $CD4^+$-Th17/Treg immune homeostasis and maintain intestinal health by regulating the expression of intestinal CD4, Foxp3 and RORγt proteins in model mice.

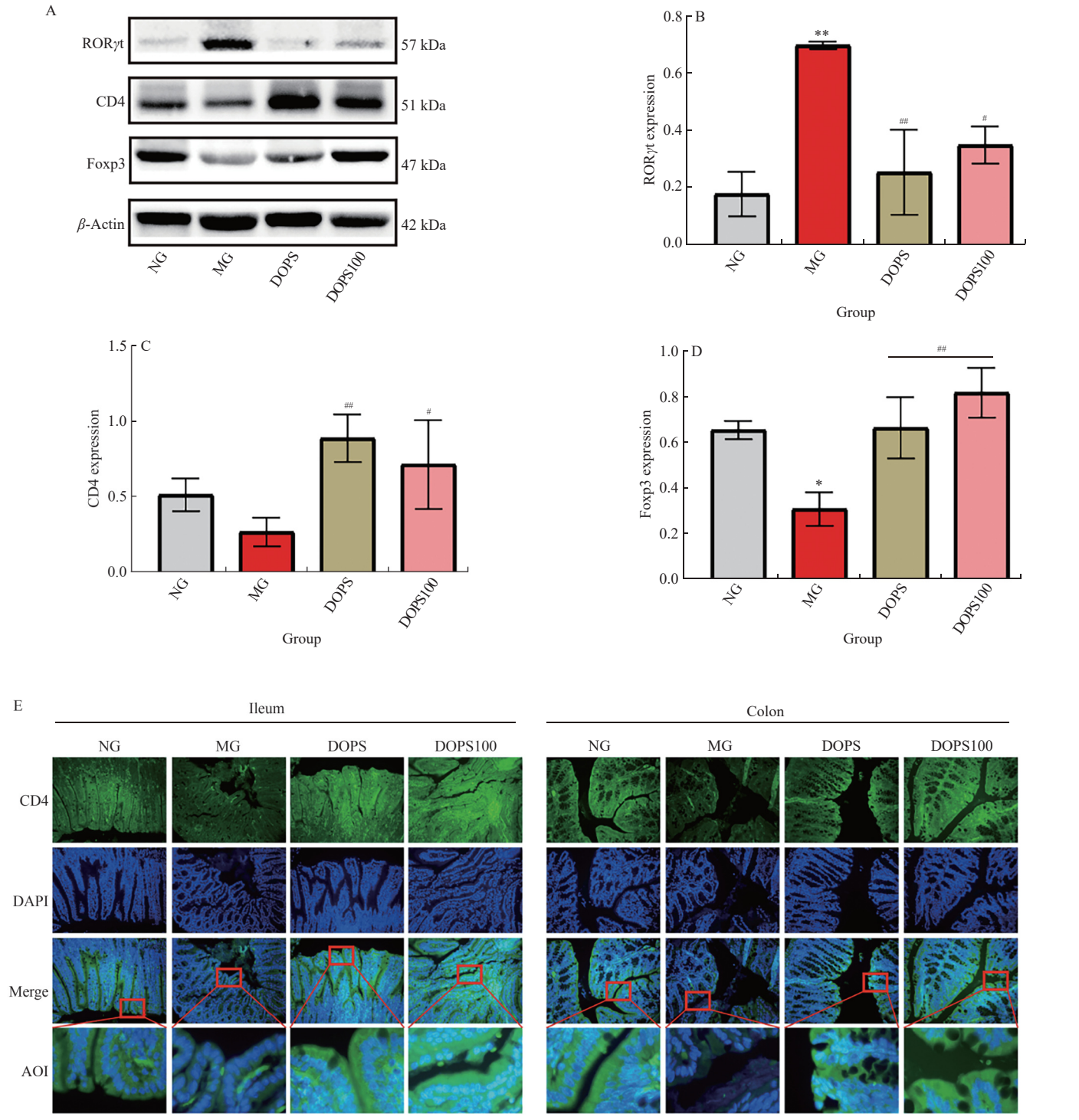

Fig. 9 Effects of DOPS and DOPS100 on reshape the $CD4^+$-Th17/Treg pathway in sub-healthy mice. (A-D) Western blot representative images and statistical charts of ileum RORγt, CD4 and Foxp3; (E) IF representative image of CD4 in the colon and ileum (400×), scale bar = 100 μm; (F) IHC representative image of Foxp3 in the colon and ileum (400×), scale bar = 100 μm; (G) IHC representative image of RORγt in the colon and ileum (400×), scale bar = 100 μm. Compared with the NG $^*P < 0.05$, $^{**}P < 0.01$; compared with the MG $^{\#}P < 0.05$, $^{\#\#}P < 0.01$.

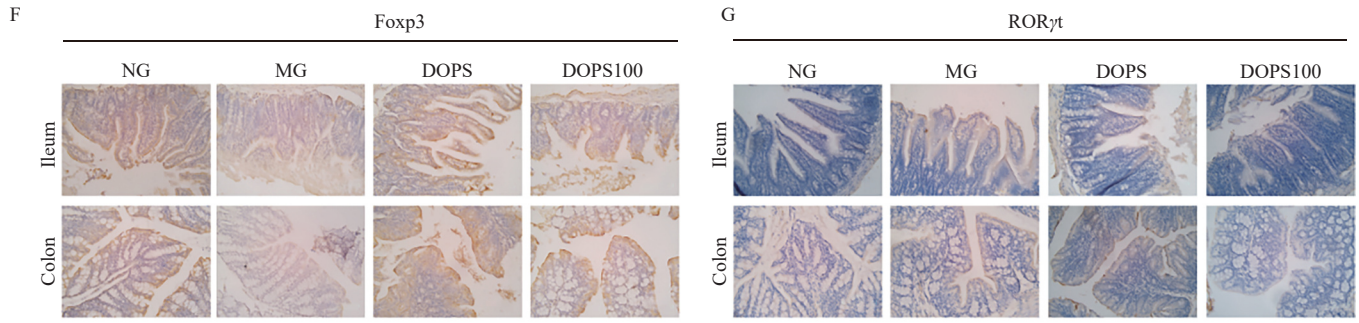

Fig. 9 (*Continued*)

3.2.7 *Effects of DOPS and DOPS100 on the expression of CD4$^+$-Th17/Treg-related cytokine proteins in sub-healthy mice*

Further studies examined on the expression of CD4$^+$-Th17/Treg-related cytokine proteins, serum and intestinal levels of IL-10, IL-22, and IL-17A, in sub-healthy mice. Compared to the normal group, intestinal the expression levels of anti-inflammatory factors of IL-10 (Figs. 10A, D, E) and IL-22 (Figs. 10C, H, I) significant decreased ($P < 0.01$, 0.05), as well as serum IL-22 (Fig. 10K). And the intestinal the expression levels of pro-inflammatory factor of IL-17A significant increased ($P < 0.01$) (Figs. 10B, F, G), as well as serum IL-17A (Fig. 10J).

Interestingly, this condition can be counteracted by DOPS and DOPS100, both of which are capable of enhancing the expression levels of intestinal anti-inflammatory factors IL-10 ($P < 0.01$, 0.05) (Figs. 10D, E) and IL-22 ($P < 0.01$) (Figs. 10H, I) proteins while reducing the expression levels of pro-inflammatory factor IL-17A ($P < 0.01$, 0.05) (Figs. 10F, G) proteins. Additionally, the levels of serum IL-22 and IL-17A ($P < 0.01$, 0.05) (Figs. 10J, K) exhibited an improvement following DOPS and DOPS100 administration. These results substantiated the DOPS and DOPS100 contributed to ameliorating intestinal inflammation and reestablishing intestinal immune homeostasis.

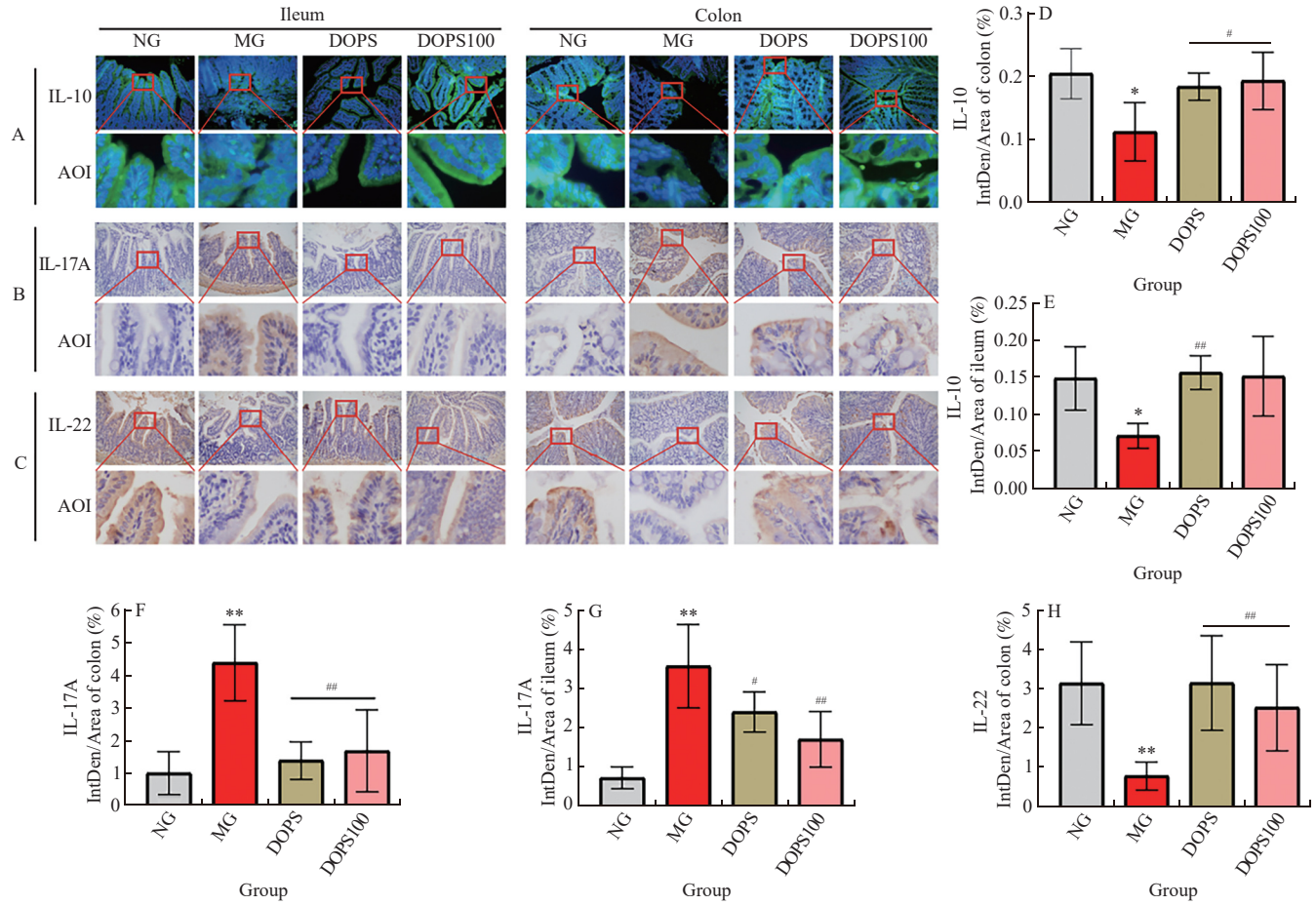

Fig. 10 Effects of DOPS and DOPS100 on the expression of CD4$^+$-Th17/Treg-related cytokine proteins in sub-healthy mice. (A, D, E) IF representative images and statistical charts of ileum IL-10 in the colon and ileum (400×), scale bar = 100 μm; (B, F, G) IHC representative image of IL-17A in the colon and ileum (400×), scale bar = 100 μm; (C, H, I) IHC representative image of IL-22 in the colon and ileum (400×), scale bar = 100 μm; (J, K) Serum IL-17A and IL-22. Compared with the NG $^*P < 0.05$, $^{**}P < 0.01$; compared with the MG $^{\#}P < 0.05$, $^{\#\#}P < 0.01$.

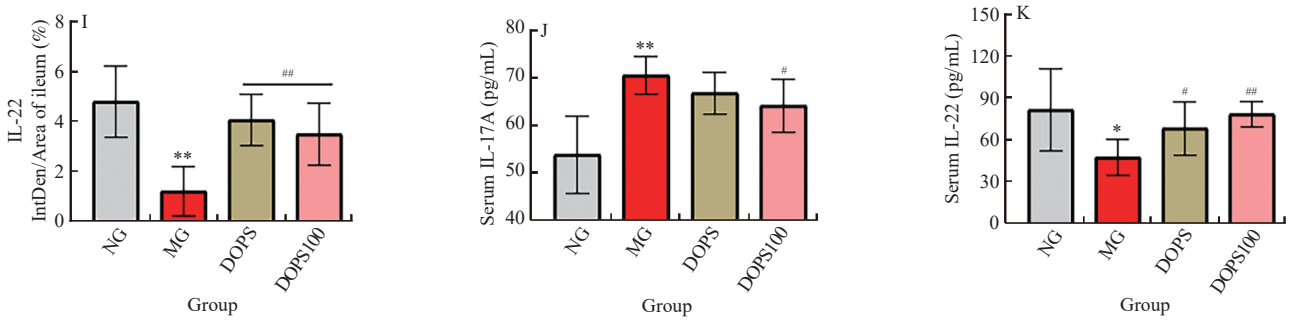

Fig. 10 (*Continued*)

4. Discussion

The crude polysaccharide (DOPS) was extracted from the ultrafine powder of *D. officinale* stems and further purified using DEAE-52 cellulose and Sephadex G100 columns to obtain DOPS100. Structural characterization of DOPS100 revealed no significant difference in the total polysaccharide content compared with DOPS and DOPS100. Polysaccharides with triple-helical structures are known for their excellent biological activities. The results of the congo red test suggest that DOPS and DOPS100 may possess good anticomplementary activities. However, DOPS100 exhibited significantly lower total glucuronides and total flavonoids than DOPS, indicating the removal of most acidic polysaccharides and total flavonoids components during the purification process. This resulted in a purer sample for subsequent *in vivo* experiments. Additionally, DOPS100 contained minimal total saponin and total phenol components, further increasing its purity for subsequent *in vivo* experiments to verify the drug efficacy.

The immunostimulatory activity of polysaccharides is closely associated with their properties such as chemical composition, glycosidic bonding, conformation, and degree of esterification[16,39]. Polysaccharides with molecular weights more than 100 kDa possess excellent immunostimulatory activity[40]. Additionally, Lu et al.[41] reported that a high content of mannose in DOP improves antitumor activity. The glucomannan-rich structure of DOPS can effectively inhibit the proliferation of pathogenic bacteria, alleviate inflammation, improve the integrity of the intestinal mucosa, and increase nutrient absorption[42].

However, although polysaccharides from different purification levels of *D. officinale* have similar composition and structural characteristics, they have different effects on bioactivity. The structural differences, such as the higher proportion of mannose monosaccharide composition and lower degree of esterification in purified DOPS100, result in significant differences in biological activity. Hence, performing a thorough investigation into the structural characteristics and mechanisms of immunoreactivity is imperative for completely understanding the structure-immunoreactivity relationship. In the present study, we performed *in vivo* experiments using an anthropomorphic poor diet-induced immunocompromised mouse model, administering DOPS and DOPS100. We found that both types of polysaccharides can improve the suboptimal health status of the model mice to different degrees, alleviating symptoms such as fatigue and abnormal metabolic indexes. Analysis of the effects of polysaccharides on the humoral and cellular immune functions of the model revealed that the poor diet led to immune organ damage[43], resulting in decreased concentrations of immunoglobulins IgA and IgM and abnormal activation of the serum complement system[44-46]. DOPS100 significantly reversed these phenomena, indicating stronger activity in cellular and humoral immunity compared with DOPS.

A well-functioning intestinal barrier is crucial for the normal functioning of all organs and systems in the human body[47-48]. The intestinal surface, which is the internal surface of the organism, exchanges complex information every day with several substances, including food components and microorganisms. It mainly depends on the intestinal barrier to decide whether these substances should enter the body. The intestinal barrier is composed of the following four parts: biological barrier, mechanical barrier, chemical barrier, and immune barrier. The mechanical barrier is composed of mucosal epithelial cells and their intercellular tight junction proteins, whereas the immune barrier is composed of intestinal tissues such as intestinal epithelial cells, lymphoid tissues, and mesenteric lymph nodes[49].

The length of the villi is significantly associated with the number of cells in their intestinal epithelium. When the villi are short, fewer mature villous cells are present and nutrient uptake is reduced. Additionally, the depth of crypts reflects the rate of cell production, and the cells continuously migrate and differentiate from the base of crypts to the end of villi to supplement the normal shedding of villous epithelium. Villous height/crypt depth the functional status of the small intestine. Furthermore, an increase in the ratio indicates an improved mucosa, digestion and absorptive function, as well as accelerated growth and development. Conversely, a decrease in the ratio suggests a decrease in the digestive and absorptive function and mucosal damage. Tight junction proteins, such as Occludin and ZO-1, contribute to the stabilization of intercellular tight junctions and optimize the intestinal barrier function. ZO-1 is crucial for effective mucosal repair. A previous study showed that polysaccharides exert their immunomodulatory activities by triggering intestinal mucosal immunity rather than being directly absorbed into the blood[50]. In the present study, we found that oral administration of DOPS and DOPS100 improved the intestinal immunity of mice by restoring abnormal intestinal villus length and crypt depth, increasing the number of intestinal mucosal cuprocytes, and remodeling the intestinal mechanical barrier through upregulated expression of intestinal tight junction proteins ZO-1 and Occludin. Altogether, DOPS100 treatment is generally better than DOPS.

$CD4^+$ T cells are important elements of immune response and immune regulation and hold immense significance in intestinal immunity. In the intestinal environment, these cells can transform into various subsets, including Treg and effector T cells such as Th17. Two important transcription factors, Foxp3 and RORγt, play crucial

roles in controlling the differentiation and functionality of Treg and Th17, respectively. The activities of these transcription factors are crucial for maintaining the balance between intestinal immunity and combating infections[51]. Alcohol consumption decreased intestinal CD4 levels, thus compromising host gut immunity[52].

Th17 can trigger different autoimmune diseases, which are crucial for host defense against extracellular pathogens. The differentiation, proliferation, and secretion of Th17 are tightly regulated by many factors, such as transforming growth factor-β (TGF-β), IL-6, IL-21, IL-23, signal transducer and activator of transcription 3 (STAT3), RORγt, and RORα. These factors facilitate the differentiation of $CD4^+$ T cells into Th17[53]. Th17 produce many transcription factors, such as IL-17A, IL-17F, IL-22, and IL-21, exerting predominantly proinflammatory effects[54-56]. $CD4^+$ Treg, the most prevalent type currently studied, promote differentiation via STAT5 and Foxp3, and exert immunomodulatory functions via direct cell-to-cell contact inhibition, secretion of inhibitory cytokines (such as IL-10 and TGF-β), and induction of apoptosis[57-59].

Western blotting and IHC analyses showed a significant reduction in the protein levels of CD4, Foxp3, IL-10, and IL-22 in the gut, accompanied by a notable increase in the protein levels of RORγt and IL-17A. This suggests that a poor diet may affect the $CD4^+$-Foxp3/RORγt immune axis. The dysregulation of this immune axis inhibits the activation of Treg, compromising the secretion of anti-inflammatory cytokines and promoting an increase in the autoimmune response of Th17. Consequently, the excessive secretion of proinflammatory factors induces disturbances in intestinal immune function. Further experimentation showed that DOPS and DOPS100 suppressed the proliferation and differentiation of Th17 within the intestinal mucosa of the model mice. Additionally, these compounds improved the immunomodulatory abilities of Treg, thus shifting the intestinal $CD4^+$-Foxp3/RORγt immune axis towards equilibrium. Further improvements in the aberrant expression of anti-inflammatory and proinflammatory factors resulting from the excessive consumption of fatty glycol wine were observed. This finding reveals the potential of DOPS to regulate intestinal immune balance by modulating the intestinal $CD4^+$-Foxp3/RORγt signaling pathway in model mice[60-61].

5. Conclusion

The DOPS100 and DOPS exert excellent benefits on the health status and immunity of immunocompromised model mice induced by poor dietary habits. This was evidenced by the improvement in general symptoms of suboptimal health, improvement of humoral and cellular immune functions in the model mice, increase in intestinal immune $CD4^+$ T cells and Treg, increase in anti-inflammatory factors IL-10 and IL-22, and decrease in proinflammatory factor IL-17A. Furthermore, DOPS and DOPS100 could remodel the intestinal barrier and restore intestinal $CD4^+$-Th17/Treg immune homeostasis via intestinal immunity. The novelty of this study lies in elucidating the mechanism underlying DOPS in improving immunity via gut-immune homeostasis.

Altogether, the results confirmed the immunoregulatory properties of DOPS, highlighting the potential for research and development of functional foods and pharmaceuticals derived from *D. officinale*. DOPS100 exerted superior activities compared with DOPS. Nevertheless, additional research is warranted to elucidate the mechanisms by which DOPS are absorbed and utilized in the intestine. Furthermore, how they modulate the suboptimal health states of the body through their effects on intestinal homeostasis should be investigated.

Ethics statement

The study method and treatment procedure were considered and approved by the ethics committee of Zhejiang University of Technology (MG20220923012).

Conflict of interest

The authors declare that they have no competing interests.

Acknowledgements

This research was supported by the National Natural Science Foundation of China (82274134) and the National Key R&D Plan (2017YFC1702200, 2017YFC1702202) and Key R&D Program Projects in Zhejiang Province (2020C04020) and the Key Research and Development Program of Zhejiang Province (2025C02183).

Data availability statement

The data used to support the findings of this study are available from the researchers upon request.

References

[1] C. Luo, X. Xu, X. Wei, et al., Natural medicines for the treatment of fatigue: bioactive components, pharmacology, and mechanisms, Pharmacol. Res. 148 (2019) 104409. https://doi.org/10.1016/j.phrs.2019.104409.

[2] M. Shi, M. Yan, J. Su, et al., Effects of *Dendrobium officinale* ultrafine powder on sub-health mice induced by unhealthy lifestyle based on neuroendocrine immune system, Food Funct. 13 (2022) 12436-12450. https://doi.org/10.1039/D2FO02158G.

[3] H. Chen, Y. Fu, X. Jiang, et al., Arabinoxylan activates lipid catabolism and alleviates liver damage in rats induced by high-fat diet, J Sci Food Agric. 98 (2018) 253-260. https://doi.org/10.1002/jsfa.8463.

[4] F.E. García-Arroyo, G. Gonzaga-Sánchez, E. Tapia, et al., Osthol ameliorates kidney damage and metabolic syndrome induced by a high-fat/high-sugar diet, Int. J. Mol. Sci. 22 (2021) 2431. https://doi.org/10.3390/ijms22052431.

[5] K. Aso, M. Kono, M. Kanda, et al., Itaconate ameliorates autoimmunity by modulating T cell imbalance via metabolic and epigenetic reprogramming, Nat. Commun. 14 (2023) 984. https://doi.org/10.1038/s41467-023-36594-x.

[6] X. Chen, M.C. Berin, V.L. Gillespie, et al., Treatment of intestinal inflammation with epicutaneous immunotherapy requires TGF-β and IL-10 but not Foxp3+ Tregs, Front Immunol. 12 (2021) 637630. https://doi.org/10.3389/fimmu.2021.637630.eCollection 2021.

[7] S. Xing, W. Yu, X. Zhang, et al., Isoviolanthin extracted from *Dendrobium officinale* reverses TGF-β1-mediated epithelial-mesenchymal transition in hepatocellular carcinoma cells via deactivating the TGF-β/Smad and PI3K/Akt/mTOR signaling pathways, Int. J. Mol. Sci. 19 (2018) 1556. https://doi.org/10.3390/ijms19061556.

[8] Y. Liu, L. Yang, Y. Zhang, et al., *Dendrobium officinale* polysaccharide ameliorates diabetic hepatic glucose metabolism via glucagon-mediated signaling pathways and modifying liver-glycogen structure, J. Ethnopharmacol. 248 (2020) 112308. https://doi.org/10.1016/j.jep.2019.112308.

[9] X. Gao, T. Ye, Y. Lei, et al., *Dendrobium officinale* aqueous extract influences the immune response following vaccination against SARS-CoV-2, Biomed. Pharmacother. 162 (2023) 114702. https://doi.org/10.1016/j.biopha.2023.114702.

[10] J. Chen, Essential role of medicine and food homology in health and wellness, Chin. Herb Med. 15 (2023) 347-348. https://doi.org/10.1016/j.chmed.2023.05.001.

[11] X. Gu, D. Hao, P. Xiao, Research progress of Chinese herbal medicine compounds and their bioactivities: fruitful 2020, Chin. Herb Med. 14 (2022) 171-186. https://doi.org/10.1016/j.chmed.2022.03.004.

[12] M. Li, H. Yue, Y. Wang, et al., Intestinal microbes derived butyrate is related to the immunomodulatory activities of *Dendrobium officinale* polysaccharide, Int. J. Biol. Macromol. 149 (2020) 717-723. https://doi.org/10.1016/j.ijbiomac.2020.01.305.

[13] X. Huang, S. Nie, H. Cai, et al., Study on *Dendrobium officinale O*-acetylglucomannan (dendronan): part IV. immunomodulatory activity *in vivo*, J. Funct. Foods 15 (2015) 525-532. https://doi.org/10.1016/j.jff.2015.03.054.

[14] J. Li, W. Tao, W. Zhou, et al., *Dendrobium officinale* leaf polysaccharide has a dual effect of alleviating the syndromes of immunosuppressed mice and modulating immune system of normal mice, J. Funct. Foods 113 (2024) 105974. https://doi.org/10.1016/j.jff.2023.105974.

[15] X.F. Liu, J. Zhu, S.Y. Ge, et al., Orally administered *Dendrobium officinale* and its polysaccharides enhance immune functions in BALB/c mice, Nat. Prod. Commun. 6 (2011) 867-870.

[16] S.Z. Xie, B. Liu, D.D. Zhang, et al., Intestinal immunomodulating activity and structural characterization of a new polysaccharide from stems of *Dendrobium officinale*, Food Funct. 7 (2016) 2789-2799. https://doi.org/10.1039/C6FO00172F.

[17] Y.J. Dong, M.Q. Lin, X. Fang, et al., Modulating effects of a functional food containing *Dendrobium officinale* on immune response and gut microbiota in mice treated with cyclophosphamide, J. Funct. Foods 94 (2022) 105102. https://doi.org/10.1016/j.jff.2022.105102.

[18] H.L. Xie, J.Y. Fang, M.A. Farag, et al., *Dendrobium officinale* leaf polysaccharides regulation of immune response and gut microbiota composition in cyclophosphamide-treated mice, Food Chem. X 13 (2022) 100235. https://doi.org/10.1016/j.fochx.2022.100235.

[19] S. Feng, W. Liu, S. Zuo, et al., Impaired function of the intestinal barrier in a novel sub-health rat model, Mol. Med. Rep. 13 (2016) 3459-3465. https://doi.org/10.3892/mmr.2016.4978.

[20] Y. Tong, H. Gao, Q. Qi, et al., High fat diet, gut microbiome and gastrointestinal cancer, Theranostics 11 (2021) 5889-5910. https://doi.org/10.7150/thno.56157.

[21] W. Yang, Z. Yang, Y. Zou, et al., Extraction and deproteinization process of polysaccharide from purple sweet potato, Chem. Bio. Drug Des. 99 (2022) 111-117. https://doi.org/10.1111/cbdd.13935.

[22] D. Khatri, S.B.B. Chhetri, Reducing sugar, total phenolic content, and antioxidant potential of Nepalese plants, Biomed. Res. Int. 2020 (2020) 7296859. https://doi.org/10.1155/2020/7296859.

[23] X. Sun, H. Wang, X. Han, et al., Fingerprint analysis of polysaccharides from different *Ganoderma* by HPLC combined with chemometrics methods, Carbohydr. Polym. 114 (2014) 432-439. https://doi.org/10.1016/j.carbpol.2014.08.048.

[24] A.V. Cebin, D. Komes, M.C. Ralet, Development and validation of HPLC-DAD method with pre-column PMP derivatization for monomeric profile analysis of polysaccharides from agro-industrial wastes, Polymers 14 (2022) 544. https://doi.org/10.3390/polym14030544.

[25] R. Chen, W. Li, Z. Qiu, et al., Ischemic postconditioning-mediated DJ-1 activation mitigate intestinal mucosa injury induced by myocardial ischemia reperfusion in rats through Keap1/Nrf2 pathway, Front. Mol. Biosci. 8 (2021) 655619. https://doi.org/10.3389/fmolb.2021.655619. eCollection 2021.

[26] Y.W. Chang, T.J. Lu, Molecular characterization of polysaccharides in hot-water extracts of *Ganoderma lucidum* fruiting bodies, J. Food Drug Anal. 12 (2020) 2662. https://doi.org/10.38212/2224-6614.2662.

[27] W. Wei, L. Feng, W.R. Bao, et al., Structure characterization and immunomodulating effects of polysaccharides isolated from *Dendrobium officinale*, J. Agric. Food Chem. 64 (2016) 881-889. https://doi.org/10.1021/acs.jafc.5b05180.

[28] Q. Luo, Z. Tang, X. Zhang, et al., Chemical properties and antioxidant activity of a water-soluble polysaccharide from *Dendrobium officinale*, Int. J. Biol. Macromol. 89 (2016) 219-227. https://doi.org/10.1016/j.ijbiomac.2016.04.067.

[29] H. Li, X. Gong, Z. Wang, et al., Multiple fingerprint profiles and chemometrics analysis of polysaccharides from *Sarcandra glabra*, Int. J. Biol. Macromol. 123 (2019) 957-967. https://doi.org/10.1016/j.ijbiomac.2018.11.103.

[30] R. Zhu, X. Zhang, Y. Wang, et al., Characterization of polysaccharide fractions from fruit of *Actinidia arguta* and assessment of their antioxidant and antiglycated activities, Carbohydr. Polym. 210 (2019) 73-84. https://doi.org/10.1016/j.carbpol.2019.01.037.

[31] P. Zhao, X. Li, Y. Wang, et al., Characterisation and saccharide mapping of polysaccharides from four common *Polygonatum* spp., Carbohydr. Polym. 233 (2020) 115836. https://doi.org/10.1016/j.carbpol.2020.115836.

[32] M. Chylińska, M. Szymańska-Chargot, A. Zdunek, FT-IR and FT-Raman characterization of non-cellulosic polysaccharides fractions isolated from plant cell wall, Carbohydr. Polym. 154 (2016) 48-54. https://doi.org/10.1016/j.carbpol.2016.07.121.

[33] B. Busato, E.C. de Almeida Abreu, C.L. de Oliveira Petkowicz, et al., Pectin from *Brassica oleracea* var. *italica* triggers immunomodulating effects *in vivo*, Int. J. Biol. Macromol. 161 (2020) 431-440. https://doi.org/10.1016/j.ijbiomac.2020.06.051.

[34] G.E. Do Nascimento, S.M.B. Winnischofer, M.I. Ramirez, et al., The influence of sweet pepper pectin structural characteristics on cytokine secretion by THP-1 macrophages, Food Res. Int. 102 (2017) 588-594. https://doi.org/10.1016/j.foodres.2017.09.037.

[35] Y. Duan, Z. Hu, L. Jin, et al., Isolation, characterization and anticomplementary activity of polysaccharides from the rhizomes of *Belamcanda chinensis* (L.) DC, Chem. Biodivers. 19 (2022) e202200525. https://doi.org/10.1002/cbdv.202200525.

[36] Z. Hu, H. Zhou, J. Zhao, et al., Microwave-assisted extraction, characterization and immunomodulatory activity on RAW264.7 cells of polysaccharides from *Trichosanthes kirilowii* Maxim seeds, Int. J. Biol. Macromol. 164 (2020) 2861-2872. https://doi.org/10.1016/j.ijbiomac.2020.08.072.

[37] X. Zhang, L. Zhang, X. Xu, Morphologies and conformation transition of lentinan in aqueous NaOH solution, Biopolymers 75 (2004) 187-195. https://doi.org/10.1002/bip.20112.

[38] Z. Song, Y. Hu, L. Qi, et al., An effective and recyclable deproteinization method for polysaccharide from oyster by magnetic chitosan microspheres, Carbohydr. Polym. 195 (2018) 558-565. https://doi.org/10.1016/j.carbpol.2018.04.108.

[39] S. Xu, X. Xu, L. Zhang, Branching structure and chain conformation of water-soluble glucan extracted from *Auricularia auricula-judae*, J. Agric. Food Chem. 60 (2012) 3498-3506. https://doi.org/10.1021/jf300423z.

[40] C. Wang, L. Xu, X. Guo, et al., Optimization of the extraction process of polysaccharides from *Dendrobium officinale* and evaluation of the *in vivo* immunmodulatory activity, J. Food Process. Preserv. 42 (2018) e13598. https://doi.org/10.1111/jfpp.13598.

[41] M.K. Lu, C.H. Chao, Y.C. Hsu, Advanced culture strategy shows varying bioactivities of sulfated polysaccharides of *Poria cocos*, Int. J. Biol. Macromol. 253 (2023) 126669. https://doi.org/10.1016/j.ijbiomac.2023.126669.

[42] Y.K. Nakamura, S.T. Omaye, Metabolic diseases and pro- and prebiotics: mechanistic insights, Nutr. Metab (Lond). 9 (2012) 60. https://doi.org/10.1186/1743-7075-9-60.

[43] H. Sato, S. Takase, A. Takada, Changes in liver and spleen volumes in alcoholic liver disease, J. Hepatol. 8 (1989) 150-157. https://doi.org/10.1016/0168-8278(89)90002-0.

[44] S. Hakroush, D. Tampe, P. Korsten, et al., Complement components C3 and C4 indicate vasculitis manifestations to distinct renal compartments in ANCA-associated glomerulonephritis, Int. J. Mol. Sci. 22 (2021) 6588. https://doi.org/10.3390/ijms22126588.

[45] G. Pongratz, T. Lowin, R. Kob, et al., A sustained high fat diet for two years decreases IgM and IL-1β in ageing Wistar rats, Immun. Ageing 12 (2015) 12. https://doi.org/10.1186/s12979-015-0040-1.

[46] Y. Yang, Y. Wang, L. Zhao, et al., Chinese herbal medicines for treating ulcerative colitis via regulating gut microbiota-intestinal immunity axis, Chin. Herb Med. 15 (2023) 181-200. https://doi.org/10.1016/j.chmed.2023.03.003.

[47] M. Sylvestre, S.E. Di Carlo, L. Peduto, Stromal regulation of the intestinal barrier, Mucosal. Immunol. 16 (2023) 221-231. https://doi.org/10.1016/j.mucimm.2023.01.006.

[48] K. Minton, Intestinal barrier protection, Nature Reviews. Immunology 22 (2022) 144-145. https://doi.org/10.1038/s41577-022-00685-5.

[49] L.W. Peterson, D. Artis, Intestinal epithelial cells: regulators of barrier function and immune homeostasis, Nat. Rev. Immunol. 14 (2014) 141-153. https://doi.org/10.1038/nri3608.

[50] F. Xie, K. Sakwiwatkul, C. Zhang, et al., *Atractylodis macrocephalae* Koidz. polysaccharides enhance both serum IgG response and gut mucosal immunity, Carbohydr. Polym. 91 (2013) 68-73. https://doi.org/10.1016/j.carbpol.2012.07.083.

[51] M.E. Mickael, S. Bhaumik, R. Basu, Retinoid-related orphan receptor RORγt in $CD4^+$ T-cell-mediated intestinal homeostasis and inflammation, Am. J. Pathol. 190 (2020) 1984-1999. https://doi.org/10.1016/j.ajpath.2020.07.010.

[52] F.M. Souza-Smith, L. Simon, R. Siggins, et al., Alcohol-Induced mesenteric lymphatic permeability: link to immunometabolic modulation of perilymphatic adipose tissue, Int. J. Mol. Sci. 20 (2019) 4097. https://doi.org/10.3390/ijms20174097.

[53] M.J. McGeachy, K.S. Bak-Jensen, Y. Chen, et al., TGF-β and IL-6 drive the production of IL-17 and IL-10 by T cells and restrain T(H)-17 cell-mediated pathology, Nat. Immunol. 8 (2007) 1390-1397. https://doi.org/10.1038/ni1539.

[54] P. Miossec, J.K. Kolls, Targeting IL-17 TH17 cells in chronic inflammation, Nat. Rev. Drug Disc. 11 (2012) 763-776. https://doi.org/10.1038/nrd3794.

[55] S. Zhang, The role of transforming growth factor β in T helper 17 differentiation, Immunology 155 (2018) 24-35. https://doi.org/10.1111/imm.12938.

[56] V. M, Interleukin 17 is a chief orchestrator of immunity, Nat. Immunol. 18 (2017) 612-621. https://doi.org/10.1038/ni.3742.

[57] Y. Xia, X. Fang, X. Dai, et al., Iguratimod ameliorates nephritis by modulating the Th17/Treg paradigm in pristane-induced lupus, Int. Immunopharmacol. 96 (2021) 107563. https://doi.org/10.1016/j.intimp.2021.107563.

[58] M.J. Lee, A.M. Geller, N.C. Bamford, et al., Deacetylation of fungal exopolysaccharide mediates adhesion and biofilm formation, mBio. 7 (2016) e00252-00216. https://doi.org/10.1128/mBio.00252-16.

[59] C.G. Mayne, C.B. Williams, Induced and natural regulatory T cells in the development of inflammatory bowel disease, Inflamm. Bowel Dis. 19 (2013) 1772-1788. https://doi.org/10.1097/MIB.0b013e318281f5a3.

[60] G. Liu, K. Gu, X. Liu, et al., Dietary glutamate enhances intestinal immunity by modulating microbiota and Th17/Treg balance-related immune signaling in piglets after lipopolysaccharide challenge, Food Res. Int. 166 (2023) 112597. https://doi.org/10.1016/j.foodres.2023.112597.

[61] M. Zou, Y. Wang, Y. Liu, et al., Huangshan floral mushroom polysaccharide ameliorates dextran sulfate sodium-induced colitis in mice by modulating Th17/Treg balance in a gut microbiota-dependent manner, Mol. Nutr. Food Res. 67 (2023) 2200408. https://doi.org/10.1002/mnfr.202200408.